A New Sidelobe Reduction Method for Circular SAR

Gaowei Jia, Wenge Chang, and Ruibin Tu
College of Electronic Science and Engineering
National University of Defense Technology, Changsha, Hunan 410073, China

Abstract— Circular synthetic aperture radar (CSAR) has become of particular interest to the SAR community. According to the isotropic targets, the spectrum of which is ring-shaped, therefore the corresponding point spread function (PSF) is related to Bessel Function, and the sidelobe level is higher. In this paper, a novel sidelobe reduction method based on the image processing is proposed. Simulation test proved that this method could express the sidelobe of CSAR from −8 dB to −16 dB without the expansion of mainlobe.

1. INTRODUCTION

Circular synthetic aperture radar (CSAR) has become the hotspot in the SAR community in recent years [1, 2], However, the higher sidelobe level would limit its application. For isotropic targets, the spectrum of which is ring-shaped therefore the corresponding point spread function (PSF) is related to Bessel function, thus the corresponding sidelobe level is much higher than that of linear-trajectory SAR. Moreover, the traditional window-function technique is not valid any more and yields even worse results for CSAR. Thus it is essential to develop new methods to reduce the sidelobe level for CSAR.

It is learnt from the theory of Fourier-based imaging that [3]: firstly, the discontinuity of the spectrum leads to the emergence of sidelobes of the PSF. Secondly, the direction of the sidelobe of the PSF is perpendicular to the edge of the spectrum. These two factors could be used to explain why the sidelobe directions according to CSAR displayed radially. Specifically, the fundamental motivation of the proposed sidelobe reduction method is to extract the sidelobe-image firstly and then deducting it to obtain the sidelobe-compressed CSAR images.

2. THE ANALYSIS OF THE SPECTRUM SHAPE OF CSAR

The geometry of circular SAR system is shown in Fig. 1.

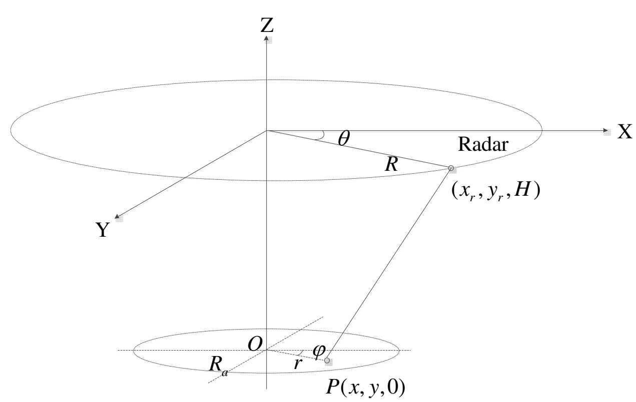

Figure 1: The geometry of circular SAR.

Figure 1 stands for the imaging geometry of CSAR. In Fig. 1, the SAR sensor moves along a circle with the radius of R, the velocity is v. $\theta \in [0, 2\pi]$ represents the aspect angle, 0 degree of θ stands for the positive x axis. O is the origin. The three dimensional (3-D) positions of the array phase center (APC) are (x_r, y_r, H), i.e., (R, θ, H) in the polar coordinates. During the movement of SAR sensor, the beam is always spotlighted on the flat observed scene (with a radius of R_a). Denoting the incident angle according to the centered target is θ_z. P is an arbitrary off-centered target located in the observed area with the 3-D positions of $(x, y, 0)$, i.e., $(r, \varphi, 0)$ in the polar coordinates. The instantaneous range from the APC to P is

$$R_r(\theta) = \sqrt{R^2 + r^2 + H^2 - 2Rr\cos(\theta - \varphi)} \tag{1}$$

Denoting the transmitted signal is linear frequency modulation (LFM), the echo of CSAR after matched filtering in range could be expressed as

$$S(k, \theta) = \exp(-j2kR_r) \tag{2}$$

For the sake of simplify, the envelop windows in (2) is ignored. Since the PSF is closely related to the shape of 2-D spectrum of SAR [12], we have to measure the shape of the 2-D spectrum of CSAR. From Equations (1) and (2) it is known the phase history of CSAR is $\Phi = -2k\sqrt{(x - R\cos\theta_m)^2 + (y - R\sin\theta_m)^2 + H^2}$ and the wavenumber in x and y could be recalculated as

$$\begin{aligned} k_x &= \frac{\partial\Phi}{\partial x} = -2k\frac{x - R\cos\theta_m}{\sqrt{(x - R\cos\theta_m)^2 + (y - R\sin\theta_m)^2 + H^2}} \\ k_y &= \frac{\partial\Phi}{\partial y} = -2k\frac{y - R\sin\theta_m}{\sqrt{(x - R\cos\theta_m)^2 + (y - R\sin\theta_m)^2 + H^2}} \end{aligned} \tag{3}$$

in which k_x and k_y stand for the wavenumber in x and y, respectively. Assuming $\rho = \sqrt{k_x^2 + k_y^2}$ represents the radial wavenumber in the ground plane, we have

$$\rho(\phi) = \frac{\sqrt{(x - R\cos\theta)^2 + (y - R\sin\theta)^2}}{\sqrt{(x - R\cos\theta)^2 + (y - R\sin\theta)^2 + H^2}} \tag{4}$$

in which $\phi = \tan^{-1}(k_x/k_y)$, the value of $\rho(\phi)$ determines the shape of the 2D spectrum in the ground plane. It is seen from Equation (26) that the value of ρ is dependent on the position of target, i.e., the shapes of spectrum according to different targets are space-variant. For centered isotropic target, $\rho = 2k\cos\theta_z$, denoting the spectrum is standard ring-shaped. For off-centered isotropic targets, the spectrum is no longer standard ring-shaped. Specifically, taking the edged target $(R_a, 0, 0)$ for example, the corresponding maximum and minimum value of ρ are

$$\rho_{\min} = 2k\frac{R - R_a}{\sqrt{(R - R_a)^2 + H^2}}, \quad \rho_{\max} = 2k\frac{R + R_a}{\sqrt{(R + R_a)^2 + H^2}} \tag{5}$$

Denoting η is a ratio to represent the relative shift of the radial wavenumber:

$$\eta = \max\left\{\frac{|\rho_{\max} - \rho|}{\rho}, \frac{|\rho_{\min} - \rho|}{\rho}\right\} \tag{6}$$

in which $|\cdot|$ stands for the absolute value. When $\eta = 0$, the 2-D spectrum is standard ring-shaped, otherwise the 2-D spectrum is no longer standard ring-shaped. Moreover, larger value of η denotes a more distorted ring shape. To have a better insight, numerical analysis is carried out. The parameters of CSAR are listed in Table 1.

Table 1: Parameters for numerical analysis.

Carrier frequency	10 GHz	Radius of the observed scene	40 m
Bandwidth	600 MHz	Height of track	500 m
Radius of the circular track	1000 m	Velocity of carrier	40 m/s

In Table 1 it is noted that the observed area is smaller than that of strip-mode SAR. For one thing, the beam width of high waveband CSAR is narrow, thus the observed area is small. For another, the incredible trajectory derivation would make the observed area smaller. Based on the parameters shown in Table 1, the corresponding η according to the edged point target is 0.0084, denoting the shift distortion is too small so that the 2-D spectrum of all the off-centered isotropic targets could be seen as the standard ring in the domain of (k_x, k_y).

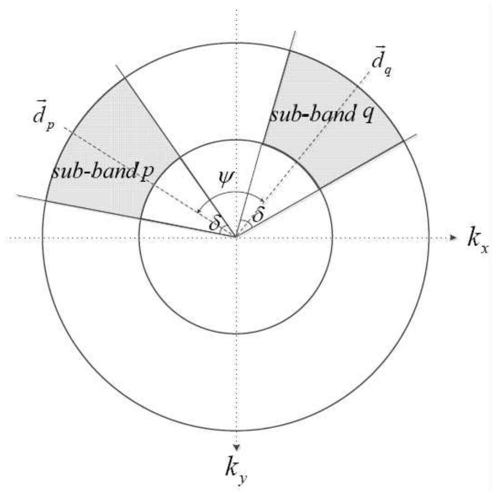

Figure 2: The shape of the spectrum of CSAR.

3. THE EXTRACTION OF SIDELOBE IMAGES

According to the isotropic target, the corresponding ring-shaped 2-D spectrum could be expressed in Fig. 2.

In Fig. 2, it is assumed that there are two arbitrary sub-spectrums p and q which have the same aspect width δ. The differential angle between them is ψ. $\vec{d_p}$ and $\vec{d_q}$ stand for the directions of the central aspect angle of sub-spectrums p and q, respectively.

Based on the Fourier-based imaging theory, it is learnt the PSFs according to sub-spectrum p and q have the same location and width of the mainlobe, but possess different directions of sidelobe. The difference between the sub-images of these two sub-spectrums p and q could cancel the mainlobe image and keep the sidelobe image.

Specifically, to decrease the overlap between the sidelobes according to these two sub-spectrums, i.e., to keep the sidelobe image as far as possible, $\vec{d_p}$ and $\vec{d_q}$ are expected to be orthogonal. On the other hand, to eliminate the mainlobe during the difference of sub-images as far as possible, the aspect width of sub- spectrum is expected to be larger. Therefore, the optimal selections of ϕ and ψ are suggested as

$$\delta = \pi/2, \quad \psi = \pi/2 \tag{7}$$

Based on (7), quartering of the whole spectrum is adopted to obtain the sidelobe image. However, the extraction based on (7) still suffers the loss of sidelobe image because the intrinsic coupling between two arbitrary sub-spectrums is inevitable to cause overlapped sidelobes. To limit the degradation of sidelobe image, an available method is segmenting the whole spectrum with different quartering. Then adopt the incoherent averaging of different sidelobe images as the final sidelobe image.

Figure 3 shows two different partitions of the spectrum. In Fig. 3(a) the sub images according to sub-spectrums 1–4 are named as I_1, I_2, I_3, I_4. The corresponding sidelobe-image is obtained by:

$$I_s = ||I_1| - |I_2|| + ||I_3| - |I_4|| \tag{8}$$

where $|\cdot|$ stands for the absolute value. Similarly, the subimages corresponding to the sub-spectrums 1–4 shown in Fig. 3(b) are named as I_{1a}, I_{2a}, I_{3a}, I_{4a}, the extracted sidelobe-image is

$$I_{sa} = ||I_{1a}| - |I_{2a}|| + ||I_{3a}| - |I_{4a}|| \tag{9}$$

Theoretically, other sidelobe images can be obtained by different quartering partition. However, it does not make sense to gain limited improvement with much more computation. Therefore, only two different quartering partition, shown in Figs. 3(a) and (b), are performed in this paper to get the finial sidelobe image. The incoherent averaging of I_s and I_{sa} is

$$\tilde{I}_s = \frac{1}{2}\left(I_s + I_{sa}\right) \tag{10}$$

Figure 3: Two different partitions of spectrum.

Given the CSAR image according to the whole spectrum is I_0. Then the magnitude image after the sidelobe reduction is

$$I_m = \left| |I_0| - \tilde{I}_s \right| \tag{11}$$

4. SIMULATION TEST

According to edged target (40 m,0,0), the corresponding sidelobe images produced with the partitions shown in Figs. 3(a) and (b) are depicted in Figs. 4(a) and (b), respectively.

In addition, Fig. 4(c) denotes the incoherent averaging of sidelobe images shown in Figs. 4(a) and (b). The vertical and horizontal axes of the contour shown in Figs. 4(a)–(c) are defined as x axis and y axis, respectively. Fig. 4(d) represents the 3-D presentation of the sidelobe-image shown in Fig. 4(c). Intuitively, the sidelobe image point target (40 m,0,0) is obtained. In Fig. 4(e), the presentation of the PSF according to the whole-aperture spectrum is presented [4]. After subtracting the obtained sidelobe image shown in Fig. 4(d), we could obtain the result of sidelobe reduction, as shown in Fig. 4(f). To have a better insight, the profiles of PSF shown in Figs. 4(e) and (f) are obtained and shown in Fig. 5.

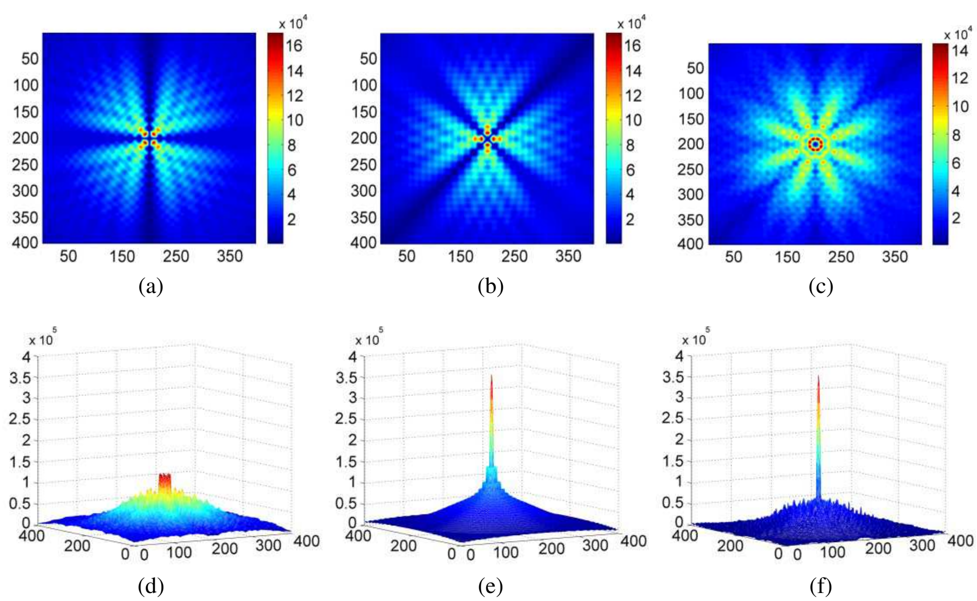

Figure 4: Simulation results, (a) and (b) denote sidelobe images, (c) and (d) are the incoherent averaging results of sidelobe images, (e) and (f) are the PSF before and after sidelobe reduction.

Figures 5(a) and (b) stand for the profiles of PSF in x and y, respectively. In addition, the quantitive measurements, contain the -3 dB resolution, peak-to-sidelobe ratio (PSLR), 2-D integral sidelobe ratio (ISLR), are calculated and listed in Table 2.

Table 2: The quantitive measurement of the imaging results.

Measurement	Without SLR	With SLR
-3 dB resolution in x (m)	0.006	0.006
PSLR in x	-7.95 dB	-16 dB
-3 dB resolution in y (m)	0.006	0.006
PSLR in y	-7.96 dB	-16.2 dB
2-D ISLR	10.22 dB	4.27 dB

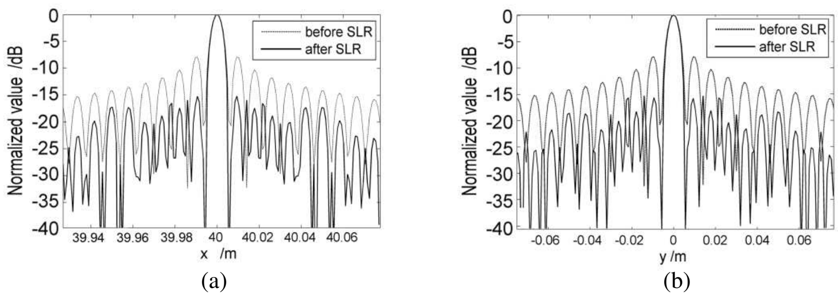

Figure 5: Results of sidelobe reduction (a) profiles in x, (b) profiles in y.

It is seen from Fig. 5 and Table 2 that after the sidelobe reduction, the mainlobe of the PSF is preserved very well. Moreover, the PSLR reduces from -7.95 dB to -16 dB, and 2D integrated sidelobe ratio (ISLR) reduces from 10.22 dB to 4.27 dB. The imaging results shown in Figs. 4 and 5 represent that the proposed method is available to reduce the sidelobe level to a large extent. The proposed sidelobe reduction method is flexible to be implemented: it can be performed within the imaging flow and also could be considered as the post-processing of the complex CSAR image.

5. CONCLUSION

A method of reducing the sidelobe level is proposed in this paper. Firstly, partition of the CSAR spectrum is proposed, based on which the sub-images as well as the sidelobe image are obtained. Subtracting the sidelobe image from the former CSAR image yields the sidelobe-reduced CSAR image. Simulation test verified the feasibility of the proposed method.

REFERENCES

1. Soumekh, M., *Synthetic Aperture Radar Signal Processing with Matlab Algorithms*, John Wiley & Sons, Inc., New York, NY, 1999.
2. Ishimaru, A., T. K. Chan, and Y. Kuga, "An imaging technique using confocal circular synthetic aperture radar," *IEEE Trans. Geosci. Remote Sens.*, Vol. 36, No. 5, 1524–1530, 1998.
3. Carrara, W. G., R. S. Goodman, and R. M. Majewski, *Spotlight Synthetic Aperture Radar Signal Processing Alogrithms*, Artch House, Boston, London, 1995.
4. Jia, G. W. and W. G. Chang, "Modified back projection reconstruction for circular FMCW SAR," *International Radar Conference 2014*, Oct. 13–17, 2014.